 doi.org/10.1016/j.ijrmms.2020.104473

Numerical analysis of dual porosity coupled thermo-hydro-mechanical behaviour during CO_2 sequestration in coal

Lee J. Hosking [a,b], Min Chen [a,1], Hywel R. Thomas [a]

[a] Geoenvironmental Research Centre, School of Engineering, Cardiff University, Queen's Buildings, The Parade, CF24 3AA, Cardiff, UK

[b] Now at the Department of Civil and Environmental Engineering, Brunel University London, Kingston Lane, Uxbridge, Middlesex, UB8 3PH, UK

Abstract

This study presents a coupled dual porosity thermal-hydraulic-mechanical (THM) model of non-isothermal gas flow during CO_2 sequestration in coal seams. Thermal behaviour is part of the disturbed physical and chemical condition of a coal seam caused by CO_2 injection, and must be understood for accurate prediction of CO_2 flow and storage. A new porosity-permeability model is included for consideration of the fracture-matrix compartment interaction. The new model is verified against an analytical solution and validated against experimental measurements, before being used to analyse coupled THM effects during CO_2 sequestration in coal. A simulation of CO_2 injection at a fixed rate shows the development of a cooling region within the coal seam due to the Joule-Thomson effect, with the temperature in the vicinity of the well declining sharply before recovering slowly. The temperature disturbance further from the well is more gradual by comparison. Under the simulation conditions studied, CO_2 injection increases coal matrix porosity and decreases the porosity and permeability of the natural fracture network, especially in the vicinity of the injection well, due to adsorption-induced coal swelling. Compared with the effects of gas pressure and temperature, the matrix-fracture compartment interaction plays an important role in changes of porosity and permeability. Considering the temperature disturbance caused by CO_2 injection under the set of representative conditions studied, the coupled model can provide an insight into the associated effects on CO_2 flow and storage during its sequestration in coal seams.

***Keywords*: CO_2 sequestration; Gas flow; Coal; THM modelling; Dual porosity**

1. Introduction

CO_2 capture, utilisation and sequestration (CCUS) comprises a broad set of actions intended to reduce greenhouse gas emissions and mitigate climate change. Among the CCUS options is coal seam

[1] Corresponding author: Min Chen (ChenM24@cardiff.ac.uk)

sequestration [1, 2], which provides storage security by taking advantage of coal's preference to adsorb CO_2 and can also enhance coalbed methane (CBM) recovery, either for electricity generation or as a feedstock for hydrogen production. Clearly the use of CBM should not lead to additional CO_2 emissions, which in most cases requires further CCUS. Coal seams have an excellent potential to handle these excess emissions, since it is well established that the CO_2 adsorption capacity of coal is around two times greater than for the naturally occurring CBM, depending primarily on coal rank [3, 4]. When CO_2 is injected into a coal seam, it disturbs the pre-existing physical and chemical condition and initiates coal-gas interactions [5-7]. For the successful storage of CO_2 in coal seams, factors influencing CO_2 injectivity, storage security, and CBM displacement should be better understood, including the role of non-isothermal behaviour explored in this paper.

CO_2 injection can lead to a dynamic temperature system within the coal seam and adjacent strata, which in turn affects the gas transport and adsorption behaviour [7-10]. As gas flows from high pressure to low pressure, the average distance between molecules increases and leads to growth of the potential energy due to intermolecular attraction. Since the expansion process is adiabatic and the total energy remains constant, the increase in potential energy implies a decrease in the kinetic energy and temperature, with this phenomenon being known as Joule-Thomas cooling (JTC) [11]. Zagorščak and Thomas [8] observed that the high flow rate of CO_2 in a coal sample led to temperature drops of up to 6.8 °C during their experiments. Oldenburg [9] performed numerical simulations of CO_2 injection into depleted gas reservoirs to examine the importance of Joule-Thomson cooling, finding that the associated temperature drop can exceed 20 °C for a high injection rate into low permeability rock. Similarly, a coupled heat and mass flow model was developed by Ziabakhsh-Ganji and Kooi [12] to account for the pressure, temperature, and gas compositional influences on thermo-physical transport properties including density, viscosity, specific heat capacity, and Joule–Thomson coefficient. Whilst these studies do not concern the mechanical behaviour of coal during CO_2 sequestration, they show the importance of non-isothermal behaviour under similar conditions, which may be expected to have a broad impact on coal-gas systems considering the dependence of CO_2 sorption and coal swelling on temperature.

Coal swelling induced by CO_2 adsorption is a well-known phenomenon, which alters the stress state and pore pressure of a coal seam with consequent changes to its porosity and permeability. Experimental and theoretical studies have been performed to investigate the permeability changes of coal exposed to CO_2 and other gases, with detailed reviews provided by Pan and Connell [13]. Several authors have established coupled models to explore the thermal, hydraulic, and mechanical (THM) coupling mechanisms controlling coal seam behaviour. Qu et al. [14] presented a coupled model of non-isothermal gas flow and coal deformation to study coal permeability changes for different gas injection temperatures, while the effect of overburden was not considered. Their work focused on characterising internal and volumetric coal swelling and shrinking due to the competing influences of thermal and

sorption induced strains (i.e. the thermal expansion of coal is countered by a reduction in CO_2 sorption-swelling, and vice versa), with the latter found to be pre-dominant under the conditions considered. Non-isothermal behaviour has been considered in several other coupled models of CO_2 sequestration in coal [e.g. 6, 15], with the coal having been idealised as a single poroelastic medium when considering deformation. For example, Saliya et al. [6] used a single porosity model to investigate the influence of coal's hydro-mechanical properties (Biot coefficient, bulk modulus), Langmuir adsorption parameters, and the initial pore pressure during CO_2 injection.

In this study, a coupled THM model is presented within the framework of dual poroelastic theory. The model consists of three main components; gas seepage in the dual porosity system, thermal transport under local thermal non-equilibrium, and the thermo-poroelastic mechanical model. The nonlinear governing equations are implemented in the COMPASS model and solved using the finite element method. In particular, this work builds upon previous works on dual porosity CO_2 flow and coal deformation presented by Hosking et al. [16] and Chen et al.[17, 18]. The enhanced numerical model is verified using analytical solutions for poro-thermo-elasticity in the absence of gas adsorption, before validation is pursued using experimental measurements as a benchmark. The coupled thermo-poroelastic dual porosity model is then used to predict the thermal, hydraulic, and goemechanical response of a coal seam to CO_2 injection.

2. Model development

Coal is treated as a dual porosity rock comprised of a porous matrix and a natural fracture network. Injected CO_2 flows through the fracture network before leaking into the coal matrix blocks and becoming adsorbed on the internal surfaces. In this section, a set of governing equations describing the fluid flow, thermal transport, and mechanical behaviour is presented for compressible fluid flow in a coal seam. For the purposes of the present work, it is assumed that the model generally applies to coal seams that are depleted of water and CBM following primary production; hence, only single phase, single component flow of CO_2 is considered. It is further assumed that coal seams are homogenous and isotropic, that coal deformation is small and linearly elastic, and that the coal is in local thermal non-equilibrium (LTNE).

2.1 Thermo-poroelastic mechanical model

A thermo-poroelastic mechanical model is developed to represent the deformation behaviour of coal. The convention of positive stress and strain in tension is used in this study, however, the fluid pressure is defined as positive in compression. For quasi-static conditions, the linear momentum balance equation for a representative elementary volume of a fractured porous medium can be reduced to the equilibrium equation for total stresses [19]:

$$\sigma_{ij,j} + F_i = 0 \tag{1}$$

where σ_{ij} is the component of the total stress tensor and F_i is the component of the body force vector. Following convention, a comma followed by subscripts denotes the differential with respect to spatial coordinates and repeated indices denote a summation over the range of the indices.

The total stress can be expressed in terms of the effective stress and the average pore pressure according to Biot's effective stress law, as:

$$\sigma'_{ij} = \sigma_{ij} - \alpha_m u_m \delta_{ij} - \alpha_f u_f \delta_{ij} \tag{2}$$

where σ'_{ij} is the component of the effective stress tensor, δ_{ij} is Kronecker's delta tensor ($\delta = 1$ for $i = j, \delta_{ij} = 0$ for $i \neq j$), α_f and α_m are Biot coefficients, and u_m and u_f are pore gas pressures for the matrix and fracture continuum, respectively, given by:

$$u_\beta = Z_\beta R T_\beta c_\beta \tag{3}$$

where R is the universal gas constant, T_β is the temperature, c_β is the gas concentration, and Z_β is the gas compressibility factor. In this study, the equation of state (EoS) proposed by Peng and Robinson [20] is used to describe gas compressibility.

The constants α_f and α_m can be expressed in terms of physically measurable mechanical parameters, as [17]:

$$\alpha_f = 1 - \frac{K}{K_m} \tag{4}$$

$$\alpha_m = \frac{K}{K_m} - \frac{K}{K_s} \tag{5}$$

where $K = E/3(1-2v)$ is the bulk modulus of the fractured rock with E being Young's modulus, $K_m = E_m/3(1-2v)$ is the modulus of the coal matrix with E_m being the respective Young's modulus, which can be obtained from experiments performed on specimens that are devoid of fractures, K_s is the modulus of the solid constituent, and v is Poisson's ratio.

The stress-strain constitutive relationship is:

$$\sigma'_{ij} = 2G\varepsilon^e_{ij} + \lambda\varepsilon^e_v \delta_{ij} \tag{6}$$

where $G = E/2(1+v)$ is the shear modulus, $\lambda = Ev/(1+v)(1-2v)$ is the Lamé constant, ε^e_{ij} represents elastic deformation, and $\varepsilon^e_v = \varepsilon_{11} + \varepsilon_{22} + \varepsilon_{33}$ is the elastic volumetric strain.

The total strain, ε_{ij}, can be expressed as:

$$\varepsilon_{ij} = \varepsilon_{ij}^{e} + \frac{1}{3}\varepsilon_T \delta_{ij} + \frac{1}{3}\varepsilon_{ad}\delta_{ij} \tag{7}$$

where ε_T is the thermal expansion-induced volumetric strain and ε_{ad} is the adsorption-induced swelling strain.

For a homogeneous, isotropic and elastic medium, the strain-displacement relation is given by:

$$\varepsilon_{ij} = \frac{1}{2}\left(u_{i,j} + u_{j,i}\right) \tag{8}$$

where ε_{ij} is the component of the total stress tensor and u_i is the component of the solid displacement vector.

The thermal expansion-contraction strain is defined as:

$$\varepsilon_T = \alpha_T (T_m - T_r) \tag{9}$$

where α_T is the thermal expansion coefficient and T_r is the reference temperature.

The total adsorption-induced strain is calculated using a surface stress approach as [17, 21]:

$$\varepsilon_{ad} = -\frac{\alpha_m u_a}{K} \tag{10}$$

$$u_a = -\varphi \Gamma^{max} R T_m \ln(1 + b_L u_{\mathrm{m}}) \tag{11}$$

where u_a is the swelling stress, Γ^{max} is a Langmuir adsorption constant, representing the adsorption capacity per unit adsorption surface, φ is a constant material parameter representing the correlation between changes in the adsorption area of the matrix pore and the porosity of the matrix, and b_L is the inverse Langmuir pressure constant. In this study, Γ^{max} and φ are lumped together as a coefficient related to adsorption induced swelling and obtained by matching experimental data.

2.2 Gas transport

For coal, there are two distinct scales for fluid flow in coal, namely, flow in the fracture network and transport in the porous matrix. Despite the discontinuous (fractured) nature of coal, in accordance with the convention of dual continuum modelling, it is assumed that each of these flow patterns is continuous. Based on the treatment of flow mechanisms within the porous matrix block, dual porosity models can be grouped into at least two categories, namely, dual porosity-single permeability (DPSP) models and

dual porosity-dual permeability (DPDP) models. The key difference is that the DPSP model only considers bulk fluid flow within the fracture continuum with the porous matrix acting as a sink or source for fluid flow within the adjacent fractures. By comparison, in the DPDP model, the matrix is also assumed to be permeable [21]. The mass balance equations are derived in this section using the framework of the generalised DPDP model, whilst they can be transformed for the purposes of DPSP modelling simply by ignoring bulk flow in the matrix. Based on the principle of conservation of mass, single phase gas flow in each of the continua is defined as:

$$\frac{\partial \rho_\beta n_\beta}{\partial t} = -\nabla \cdot \left(\rho_\beta \mathbf{v}_\beta\right) + Q_{s\beta} + \omega\Gamma \tag{12}$$

where n_β is the porosity of continuum β, $\mathbf{v}_\beta$ is the gas velocity, $Q_{s\beta}$ is a gas sink-source term for adsorption-desorption, Γ represents the mass transfer between the fracture and matrix continua, and the parameter ω =-1 if $\beta = f$, otherwise ω =1.

Expanding the left-hand side of equation (12) produces:

$$\frac{\partial \rho_\beta n_\beta}{\partial t} = n_\beta \frac{\partial \rho_\beta}{\partial t} + \rho_\beta \frac{\partial n_\beta}{\partial t} \tag{13}$$

where ρ_β is the gas density in continuum β, given by:

$$\rho_\beta = M c_\beta \tag{14}$$

where M is the gas molar mass.

The temporal derivative of fluid density can be expanded to give:

$$\frac{\partial \rho_\beta}{\partial t} = \frac{\partial \rho_\beta}{\partial u_\beta}\frac{\partial u_\beta}{\partial t} + \frac{\partial \rho_\beta}{\partial T_\beta}\frac{\partial T_\beta}{\partial t} = \rho_\beta C_{c\beta}\frac{\partial u_\beta}{\partial t} - \rho_\beta \alpha_{T\beta}\frac{\partial T_\beta}{\partial t} \tag{15}$$

where $C_{c\beta} = \frac{1}{\rho_\beta}\frac{\partial \rho_\beta}{u_\beta}$ is the fluid compressibility and $\alpha_{T\beta} = -\frac{1}{\rho_\beta}\frac{\partial \rho_\beta}{T_\beta}$ is the thermal expansion coefficient.

Gas flow in the fracture network is assumed to be laminar and viscous, and is governed by Darcy's law. Neglecting gravity, this gives:

$$\mathrm{v}_\beta = -\frac{k_\beta}{\mu}\nabla u_\beta \tag{16}$$

where k_β is the permeability of continuum β and μ is the gas viscosity.

Gas storage in coal seams is typically dominated by the adsorbed phase within the porous matrix, where the majority of internal surface area is found. It is therefore assumed that no adsorbed gas is present in the fracture continuum, i.e. $Q_{sf} = 0$. The sink-source term in the matrix continuum is given by:

$$Q_{sm} = -\frac{dR_{ad}}{dt} \tag{17}$$

$$R_{ad} = M\rho_s c_s \tag{18}$$

where c_s is the adsorbed concentration and ρ_s is the coal density.

The adsorption behaviour of gas in coal is generally described by a Langmuir isotherm, as:

$$c_s = \frac{V_L b_L u_m}{b_L u_m + 1} \tag{19}$$

where V_L is the Langmuir volume constant. Considering the thermal effect, Tang and Ripepi [22] presented the following temperature dependent form of the inverse Langmuir pressure constant, b_L:

$$b_L = b_{L0} \exp\left(\frac{E_i}{RT_m}\right) \tag{20}$$

where b_{L0} is the temperature-independent Langmuir constant and E_i is the interaction energy between the adsorbate and the adsorbent.

Mass exchange between the dual continua is derived in this work based on the assumption that a quasi-steady state pore gas concentration distribution prevails in the matrix blocks. This assumption allows the inter-porosity gas transfer rate to be expressed as a linear function of the difference between the average pore gas concentration in the fracture and matrix continua [16]. Considering the geometric effect of coal matrix, the resulting mass exchange term for the pore gas component is expressed as [17, 18]:

$$\Gamma = aDM(c_f - c_m) \tag{21}$$

where a is a matrix block geometric factor and D is the gas diffusion coefficient in the coal matrix.

Generally, Arrhenius' law is used to describe the correlation between gas diffusion and temperature [23]. However, when the temperature change is not sufficiently large, the effect of temperature on gas diffusion may be regarded as negligible [23]. Therefore, to simplify the mass exchange, a constant sorption time, τ, is introduced to approximate the diffusivity of the coal matrix [e.g. 5], given as:

$$\tau = \frac{1}{aD} \tag{22}$$

2.3 Heat transfer

A LTNE approach is applied for separate parameterisation of the fractures and matrix pores, considering heat transfer between the continua linked with mass transfer. The slow rate of gas flow in the coal matrix means that the gas and solid grains achieve thermal equilibrium relatively quickly. In effect, it can be said that each continuum remains at local thermal equilibrium, with the potential for a non-equilibrium condition to exist between the continua. Several thermal responses may develop as a result of geological CO_2 sequestration [e.g. 7, 11]; notable among these are the Joule-Thomson effect and conductive heat exchange due to a difference in temperature between the injected CO_2 and the surrounding fluids and rock.

The governing equations for heat transfer through the fracture and matrix continua can be obtained by applying the principle of conservation of energy. Ignoring the heat supply due to thermal expansion of the solid skeleton, heat transfer in the fracture continuum can be written as:

$$n_f \rho_f C_{pg} \frac{\partial T_f}{\partial t} - n_f \left(\rho_{gf} C_{pg} \mu_{JT} + 1\right) \frac{\partial u_f}{\partial t} = \nabla \cdot \left(\lambda_g \nabla T_f\right) - \rho_f C_{pg} \mathbf{v}_f \cdot \left(\mu_{JT} \nabla u_f - \nabla T_f\right) - q_{fm} \tag{23}$$

and in the matrix continuum as:

$$\left(\rho_m C_{pm}\right)_{eff} \frac{\partial T_m}{\partial t} - n_m \left(\rho_m C_{pg} \mu_{JT} + 1\right) \frac{\partial u_m}{\partial t} = \nabla \cdot \left(\boldsymbol{\lambda}_{em} \nabla T_m\right) - \rho_f C_{pg} \mathbf{v}_m \cdot \left(\mu_{JT} \nabla u_m - \nabla T_m\right) + q_{fm} \tag{24}$$

where:

$$\left(\rho_m C_{pm}\right)_{eff} = \left(1 - n_m - n_f\right)\left(\rho_s C_{ps} + \rho_a C_{pa}\right) + \rho_g C_{pg}$$

$$\lambda_{em} = \left(1 - n_m - n_f\right)\left(\lambda_s + \lambda_a\right) + n_m \lambda_g$$

where C_{pg} and λ_g are the specific heat capacity and thermal conductivity of gas, C_{ps} and λ_s are the same for the coal solids, C_{pa} and λ_a are the same for adsorbed gas, ρ_a is the adsorbed phase density, μ_{JT} is the Joule–Thomson coefficient, and q_{fm} represent the heat transfer between the dual continua. C_{pg} and μ_{JT} are calculated using the Peng and Robinson EoS. Due to limited information on C_{pa} and λ_a for gas adsorption in coal, it is assumed that they are equivalent to C_{pg} and λ_g.

The heat transfer term, q_{fm}, is separated into two processes according to the main heat transfer mechanisms, namely, conduction across the fracture surfaces and advection via mass flow between the continua [24, 25]. This can be expressed mathematically as:

$$q_{fm} = h_T A_{fm}(T_f - T_m) + \Gamma C_{pg}(T_f - T_m) \tag{25}$$

where h_T is the heat transfer coefficient between the fracture and matrix continua, and A_{fm} is the interfacial fracture-matrix specific area, which can be estimated based on the geometric relation of the fractures and matrix blocks.

The first term on the right-hand side of equation (25) represents the heat exchange between the fracture and matrix continua by conduction across the fracture surfaces, and the second term represents heat transfer by advection through the mass exchange term. Both h_T and A_{fm} are important parameters influencing the fracture-matrix interactions. The heat transfer coefficient is typically calculated by harmonic averaging of the fracture and matrix thermal conductivities [25]:

$$h_{\mathrm{T}} = \frac{2\lambda_{em}\lambda_{ef}}{l\lambda_{ef} + w\lambda_{em}} \tag{26}$$

where λ_{ef} is the effective thermal conductivity of the fracture continuum; in this work, $\lambda_{ef} = \lambda_g$.

The interfacial fracture-matrix specific area can be obtained using geometrical considerations for an aperture, w, and a matrix block length, l [24]:

$$A_{fm} = \frac{4l}{(l + w)^2} \tag{27}$$

2.4 Porosity and permeability evolution

Generally, the relationship between porosity and permeability is given by the cubic law, written as:

$$\frac{k_\beta}{k_{\beta 0}} = \left(\frac{n_\beta}{n_{\beta 0}}\right)^3 \tag{28}$$

where $k_{\beta 0}$ and $n_{\beta 0}$ are the permeability and porosity at a reference state.

The porosity at the current state can be defined as:

$$n_\beta = n_{\beta 0} + \Delta n_\beta \tag{29}$$

where Δn_β is the change in porosity from the reference state.

For non-adsorbing gas flow in isothermal fractured rock, the fracture and matrix pore volume change per unit of bulk volume is due to three components [17], namely, (*i*) a change in pore volume with a change in bulk volume of the porous medium, (*ii*) a change in pore volume due to compression of the solid phase by fluid pressure occupying the pore space, and (*iii*) a change in pore volumes due to fracture-matrix interaction driven by a pressure difference between the pore regions. When adsorption and thermal effects are involved, the influence of adsorption-induced and thermal deformation should also be considered.

Recent studies have shown that the effect of deformation resulting from adsorption-induced swelling on the fracture and matrix pore volumes is characterised by both global and local strains [26]. Before global (volumetric) deformation occurs, adsorption-induced swelling is contained in the vicinity of a fracture as a local strain, whereby matrix expansion narrows the fracture opening. It is worth pointing out that when global deformation takes place, a fracture-matrix compartment interaction may still exist if there is a pressure difference between the pore regions. It is assumed that the effect of global swelling strain on porosity evolution is analogous to that of pore pressure. Considering the influence of multiple coupled processes after reaching a final equilibrium state, a porosity change can be expressed as:

$$\Delta n_f = (\alpha_f - n_f)\Delta\varepsilon_v + \frac{(\alpha_f - n_f)}{K_s}\Delta u_f - (\alpha_f - n_f)\left(\frac{1}{K_m} - \frac{1}{K_s}\right)\Delta(u_m^a - u_f) - \Delta\varepsilon_{al} \qquad (30a)$$

$$\Delta n_m = (\alpha_m - n_m)\Delta\varepsilon_v + \frac{(\alpha_m - n_m)}{K_s}\Delta u_m^a - (\alpha_f - n_f)\left(\frac{1}{K_m} - \frac{1}{K_s}\right)\Delta(u_f - u_m^a) + \Delta\varepsilon_{al} \qquad (30b)$$

where $u_m^a = u_m - u_a$, ε_v is the bulk volumetric strain, expressed as a combination of strain due to effective stress, adsorption, and thermal expansion, giving:

$$\Delta\varepsilon_v = \Delta\varepsilon_e + \Delta\varepsilon_{ad} + \Delta\varepsilon_T \qquad (31)$$

The first terms on the right-hand side of equations (30a) and (30b) represent the change in pore volume with a change in bulk volume, with the second terms representing the contribution of compression of solids. Interactions between the fracture and matrix continua are represented by the third and fourth terms; the former being due to the pressure difference and the latter due to local swelling. With small deformation, it is assumed that local swelling is linearly proportional to global swelling, as:

$$\varepsilon_{al} = \gamma\varepsilon_{ad} \qquad (32)$$

where γ is the ratio of local to global swelling, which can be obtained by matching the experimental results of coal swelling and permeability.

Substitution of equation (30) into equation (29) with rearrangement based on the assumption of small strain yields:

$$n_f = n_{f0} + \alpha_f \Delta\varepsilon_v + \frac{\alpha_f}{K_s}\Delta u_f - \alpha_f\left(\frac{1}{K_m} - \frac{1}{K_s}\right)\Delta\left(u_m^a - u_f\right) - \Delta\varepsilon_{al} \tag{33a}$$

$$n_m = n_{m0} + \alpha_m \Delta\varepsilon_v + \frac{\alpha_m}{K_s}\Delta u_m^a + \alpha_f\left(\frac{1}{K_m} - \frac{1}{K_s}\right)\Delta\left(u_m^a - u_f\right) + \Delta\varepsilon_{al} \tag{33b}$$

2.5 Governing equations

Substituting the relationships developed above into the stress equilibrium and transport equations yields a system of coupled governing equations expressed in terms of five primary variables, namely, the displacement vector ($\mathbf{u}$), the gas concentrations in the fracture (c_f) and matrix (c_m) continua, and the temperature in the fracture (T_f) and matrix (T_m) continua.

For thermo-poroelastic displacement:

$$C_{uu}d\mathbf{u} + C_{uf}dc_f + C_{um}dc_m + dT_m + d\boldsymbol{F} = \mathbf{0} \tag{34}$$

where:

$C_{\mathrm{uu}} = \boldsymbol{P}\mathbf{D}\boldsymbol{P}^{\boldsymbol{T}}$

$C_{uc_f} = \boldsymbol{P}\mathbf{I}\alpha_f Z_f R T_f$

$C_{uc_m} = -\boldsymbol{P}\mathbf{D}\mathbf{I}\frac{1}{3}\frac{\partial\varepsilon_{ad}}{\partial c_m} + \boldsymbol{P}\mathbf{I}\alpha_m Z_m R T_m$

$C_{uT_m} = -\boldsymbol{P}\mathbf{D}\mathbf{I}\frac{1}{3}\left(\frac{\partial\varepsilon_{ad}}{\partial T_m} + \varepsilon_T\right)$

where $\boldsymbol{P}$ is the strain matrix, $\mathbf{D}$ is the elasticity matrix, and $\mathbf{I} = [1,1,0]^T$ for plane strain problems and $\mathbf{I} = [1,1,1,0,0,0]^T$ for three dimensional problems.

For gas transport in the fracture continuum:

$$C_{c_f c_f}\frac{\partial c_f}{\partial t} + C_{c_f c_m}\frac{\partial c_m}{\partial t} + C_{c_f T_f}\frac{\partial T_f}{\partial t} + C_{c_f T_m}\frac{\partial T_m}{\partial t} + C_{c_f \mathrm{u}}\frac{\partial \mathbf{u}}{\partial t} = \nabla\cdot\left(K_{c_f c_f}\nabla c_f\right) + \nabla\cdot\left(K_{c_f T_f}\nabla T_f\right) + K_{c_f c_{f_f}} + K_{c_f c_{f_m}} \tag{35}$$

where:

$C_{c_f c_f} = n_f + \frac{\alpha_f u_f}{K_m}$

$$C_{c_f c_m} = -c_f \alpha_f \left(\frac{1}{K_m} - \frac{1}{K_s}\right)(Z_m R T_m - \frac{\partial u_a}{\partial c_m}) - c_f \frac{\partial \varepsilon_{al}}{\partial c_m}$$

$$C_{c_f T_f} = \frac{\alpha_f Z_f R c_f}{K_m}$$

$$C_{c_f T_m} = -c_f \alpha_f \left(\frac{1}{K_m} - \frac{1}{K_s}\right)(Z_m R c_m - \frac{\partial u_a}{\partial T_m}) - c_f \frac{\partial \varepsilon_{al}}{\partial T_m}$$

$$C_{c_f \mathrm{u}} = c_f \alpha_f \mathbf{I}^T \boldsymbol{P}$$

$$K_{c_f c_f} = c_f Z_f R T_f \frac{k_f}{\mu}$$

$$K_{c_f T_f} = {c_f}^2 Z_f R \frac{k_f}{\mu}$$

$$K_{c_f c_{f_f}} = -\frac{1}{\tau} = -K_{c_f c_{f_}m}$$

For gas transport and adsorption-desorption in the matrix continuum:

$$C_{c_m c_m} \frac{\partial c_m}{\partial t} + C_{c_m c_f} \frac{\partial c_f}{\partial t} + C_{c_m T_m} \frac{\partial T_m}{\partial t} + C_{c_m T_f} \frac{\partial T_f}{\partial t} + C_{c_m \mathrm{u}} \frac{\partial \mathbf{u}}{\partial t} = \nabla \cdot \left(K_{c_m c_m} \nabla c_m\right) + \nabla \cdot \left(K_{c_m T_m} \nabla T_m\right) + K_{c_m c_{m_f}} + K_{c_m c_{m_}m} \quad (36)$$

where:

$$C_{c_m c_m} = n_m + c_m \alpha_f \left(\frac{1}{K_m} - \frac{1}{K_s}\right)\left(Z_m R T_m - \frac{\partial u_a}{\partial c_m}\right) + \rho_s \frac{\partial c_s}{\partial c_m} + c_m \frac{\partial \varepsilon_{al}}{\partial c_m}$$

$$C_{c_m c_f} = -c_m \alpha_f \left(\frac{1}{K_m} - \frac{1}{K_s}\right) Z_f R T_f$$

$$C_{c_m T_m} = c_m \alpha_f \left(\frac{1}{K_m} - \frac{1}{K_s}\right)\left(Z_m R c_m - \frac{\partial u_a}{\partial T_m}\right) + \frac{\partial c_s}{\partial T_m} + c_m \frac{\partial \varepsilon_{al}}{\partial T_m}$$

$$C_{c_m T_f} = -c_m \alpha_f \left(\frac{1}{K_m} - \frac{1}{K_s}\right) Z_f R c_f$$

$$C_{c_m \mathrm{u}} = c_m \alpha_m \mathbf{I}^T \boldsymbol{P}$$

$$K_{c_m c_m} = c_m Z_m R T_m \frac{k_m}{\mu}$$

$$K_{c_m T_m} = {c_m}^2 Z_m R \frac{k_m}{\mu}$$

$$K_{c_m c_{m_f}} = \frac{1}{\tau} = -K_{c_m c_{m_}m}$$

For heat transfer in the fracture continuum:

$$C_{T_f T_f} \frac{\partial T_f}{\partial t} + C_{T_f c_f} \frac{\partial c_f}{\partial t} = \nabla \cdot \left(K_{T_f T_f} \nabla T_f\right) + A_{T_f T_f} \nabla T_f + A_{T_f c_f} \nabla c_f + K_{T_f T_{f_f}} + K_{T_f T_{f_}m} \quad (37)$$

where:

$$C_{T_fT_f} = n_f\,\rho_f C_{pg} - n_f\left(\rho_{\mathrm{gf}} C_{pg}\mu_{JT} + 1\right) Z_f R c_f$$

$$C_{T_fc_f} = -n_f\left(\rho_{\mathrm{gf}} C_{pg}\mu_{JT} + 1\right) Z_f R T_f$$

$$K_{T_fT_f} = \lambda_g$$

$$A_{T_fT_f} = -\rho_f C_{pg}\mathbf{v}_f + \rho_f C_{pg}\mathbf{v}_f \mu_{JT} Z_f R c_f$$

$$A_{T_fc_f} = \rho_f C_{pg}\mathbf{v}_f \mu_{JT} Z_f R T_f$$

$$K_{T_fT_f_f} = -h_T A_{fm} - \Gamma_{mf} C_{pg} = -K_{T_fT_f_m}$$

For heat transfer in the matrix continuum:

$$C_{T_mT_m}\frac{\partial T_m}{\partial t} + C_{T_mc_m}\frac{\partial T_m}{\partial t} = \nabla\cdot\left(K_{T_mT_m}\nabla T_m\right) + A_{T_mT_m}\nabla T_m + A_{T_mc_m}\nabla c_f + K_{T_mT_{m_f}} + K_{T_mT_{m_m}} \quad (38)$$

where:

$$C_{T_mT_m} = \left(\rho_m C_{pm}\right)_{eff} - n_f\left(\rho_{\mathrm{gf}} C_{pg}\mu_{JT} + 1\right) Z_m R c_m$$

$$C_{T_mc_m} = -n_m\left(\rho_m C_{pg}\mu_{JT} + 1\right) Z_m R T_m$$

$$K_{T_mT_m} = \lambda_{em}$$

$$A_{T_mT_m} = -\rho_m C_{pg}\mathbf{v}_m + \rho_m C_{pg}\mathbf{v}_m \mu_{JT} Z_m R c_m$$

$$A_{T_mc_m} = \rho_f C_{pg}\mathbf{v}_m \mu_{JT} Z_m R T_m$$

$$K_{T_mT_m_f} = h_T A_{fm} + \Gamma_{mf} C_{pg} = -K_{T_mT_m_m}$$

3. Computational approach

A numerical solution of the coupled governing equations is achieved using the finite element method. The Galerkin weighted residual method is employed to spatially discretise the governing equations and an implicit mid-interval backward-difference time-stepping algorithm is used for temporal discretisation. A sequential implicit numerical approach is used to couple fluid flow with geomechanics. The solution procedure follows the works on coupled THCM behaviour for fractured porous media presented in detail by Thomas and co-workers [21, 27, 28]. Both systems of equations are simultaneously solved by iteration until convergence is achieved. Time dependent matrix and fracture properties like coal porosity and permeability are updated in each time step based on the numerical

results of the previous time step. This process continues until the specified simulation time is reached. Fig. 1 shows the implemented numerical solution procedure.

4. Model verification and validation

In the following sub-section, a verification test is used to provide confidence that the governing equations have been correctly implemented in the model, which is achieved by using an analytical solution as a benchmark. The test problem considers the coupled THM response of rock under thermal loading. This is followed by a validation test aimed at providing confidence in the ability of the proposed model to predict the behaviour of a coal-gas system based on published experimental measurements. More verification and validation tests on the developed model can be found in Chen [21].

4.1 THM response of rock under thermal loading

An analytical solution is only available for the coupled THM behaviour of a single porosity medium and so it is assumed that the fracture continuum is absent, which is realised by considering fracture porosity and permeability to be zero. This verification test considers a one-dimensional fully saturated poroelastic column restrained at its base and sides, such that only vertical (uniaxial) displacement is allowed, as shown in Fig. 2. Zero fluid pressure boundaries are imposed to the top surface, where fluid may exit freely from the column, and no flow boundaries are prescribed to both sides. A constant temperature of 273 K is applied to the top surface, the initial temperature is uniform at 323 K, the initial pressure is 0 Pa, and the initial equilibrium stress is fixed at zero. The analytical solution and parameters used in this verification test are taken from Selvadurai and Suvorov [29], as listed in Table 1.

Figs. 3 show the distributions of temperature, pore pressure and displacement along the column at selected times. It can be seen that there is a good agreement between the analytical solutions and the numerical results, which provides further confidence that the coupled model developed in this work has been accurately implemented in the COMPASS code.

4.2 Validation test for CO_2 flow and coal deformation

Pini et al. [30] performed gas injection experiments on a high volatile bituminous coal core under hydrostatic confinement. Upstream and downstream pressures were measured and are now used as benchmarks to test the validity of the model developed in this work. The coal core was 2.54 cm in diameter and 3.6 cm long and was tested for He, N_2 and CO_2 injection at pressures ranging from 1 MPa to 8 MPa under constant and varying confining pressure. In this section, the results for CO_2 injection under a constant confining pressure provide a benchmark for testing the performance of the numerical model in terms of the gas flow and coal deformation behaviour. Due to the highly heterogeneous pore

structure of coal, the permeability for fluid flow in coal seams is predominantly attributed to the fracture network, with the porous matrix typically making a negligible contribution. However, the coal matrix is predominantly micro-porous, which provides a large number of sites for gas adsorption. Hence, most gas stored in coal is adsorbed onto the surfaces of micropores and a DPSP model can reasonably be applied to describe the flow behaviour. A schematic of the coal core used by Pini et al. is shown in Fig. 4a, which can be simplified to the domain shown in Fig. 4b by taking advantage of axisymmetry.

Fig. 4b shows that no flow boundaries are used along the left- and right-hand sides of the domain. A time-dependent upstream CO_2 injection pressure is prescribed, whilst for coal deformation a vertical constraint is applied to the upstream and downstream boundaries with a constant confining stress at the right-hand boundary. The left-hand side of the domain is fixed horizontally and the initial pressure is 1 MPa in both continua. The material parameters used for this test are provided in Table 2, many of which are taken from Pini et al.[30], with Γ^{max} and φ lumped together and obtained by fitting the swelling strain, as shown in Fig. 5. The internal swelling ratio comes from calibrating against the experimental data on permeability, as shown in Fig. 6. The fracture permeability used in Table 2 was selected from experimental test on Sulcis Coal presented in the work by Pini et al. [30]. A similar value of permeability can also be found in work of Zang et al. [31].

Comparisons of transient steps recorded in the experiment with those predicted by the model are shown in Fig. 7. It can be seen that the numerical model successfully predicted the CO_2 flow dynamics in coal at the laboratory scale under the conditions considered, which provides confidence that the developed model may be applied in the simulation of CO_2 sequestration in coal.

5. Analysis of THM behaviour during CO_2 sequestration in coal

This section presents an application of the coupled model to study the non-isothermal behaviour of a 890 m deep and 5 m thick coal seam during CO_2 injection. The coal seam is assumed to be homogenous, isotropic, and axisymmetric with a radius of 200 m around the injection well, as shown in Fig. 8a. To consider the interaction between the coal seam and adjacent rock strata, an analysis region is formed that runs 25 m vertically, comprising a 10 m thick caprock, the 5 m thick coal seam, and a 10 m thick underlying stratum. The system is assumed to be dry following primary CBM production with a uniform initial gas pressure and temperature of 0.1 MPa and 313 K, respectively. The caprock and underlying stratum are considered to be impermeable. A constant stress of 21 MPa is applied to the top surface of the caprock, corresponding to an overburden density of around 2450 kg/m^3, and displacement at the lower boundary and injection well is constrained. Due to different Poisson's ratios for the rock strata and coal seam, radial stresses of 5.6 MPa and 11.2 MPa are assigned at the external boundary of the

rock strata and coal seam, respectively. For fluid flow, CO_2 is injected at a fixed injection rate of 0.2 kg/s at 313 K and it is assumed that no CO_2 permeates the caprock or underlying stratum.

The domain is discretised using 4-node isoparametric quadrilateral elements with a varying mesh size that gets finer towards the injection well, as shown in Fig. 8b. Table 3 shows the parameters used in this simulation; it is assumed that the thermophysical properties of coal and rock are constant. The ratio of local swelling to global swelling is evaluated by fitting the experimental results with parameters from the literature [17]. Analysis points are located 5 m, 20 m and 40 m radially from the injection well.

5.1 Gas pressure distribution within the coal seam

Figs. 9 and 10 show the predicted spatial and temporal changes of gas pressure in the fracture and matrix pore regions of the coal seam. Gas pressure in the fractures remains larger than in the coal matrix, although the size of this difference reduces with time and distance from the injection well. The higher transmissivity of the fractures means that gas pressure near the injection well increases rapidly, which in turn promotes mass transfer into the coal matrix. Further from the injection well, the gas pressure changes are slower and there is less distinction between the pore regions. The rate of equilibration between the pore regions strongly depends on the matrix block length, l, taken here as a relatively small value of 0.01 m. Larger values of l will generally result in a larger and more sustained pressure difference between then pore regions than can be seen in Figs. 9 and 10.

5.2 Temperature distribution within the coal seam

Similar to the discussion of gas pressure given above, thermal equilibrium between the pore regions is established relatively quickly. Fig. 11 shows a temperature drop of more than 10 K that advances into the coal seam upon CO_2 injection, despite the temperature of the injected gas being the same as the initial coal seam temperature. This change in temperature results from Joule-Thomson cooling and can have a significant impact on CO_2 injectivity since CO_2 adsorption increases as temperature reduces, which may in turn increase the magnitude of coal swelling. Fig. 12 displays the temperature variation at radial distances of 5 m, 20 m and 40 m from the injection well. As a result of the larger changes in gas pressure near to the injection well, the temperature profile in this region shows the sharpest decline and then gradually recovers as injection continues. In contrast, temperature changes further from the injection well are more gradual as a result of the smoother changes in gas pressure.

5.3 Porosity and permeability changes within the coal seam

Fig. 13 shows the loss of fracture porosity resulting from CO_2 adsorption-induced coal swelling. This porosity loss is greatest near to the injection well early in the simulation, after which it becomes more

gradual as conditions tend towards equilibrium. In contrast, Fig. 14 shows that matrix porosity increases as a result of CO_2 injection, with this change again being most apparent near to the injection well. Porosity changes occur as a result of competitive mechanisms depending on the gas pressure, temperature, and CO_2 adsorption. Whilst the increase in gas pressure can increase fracture porosity by reducing the effective stress, the temperature decrease shown in Figs. 11 and 12 has a competing effect by increasing CO_2 adsorption and coal swelling. The net effect under the simulation conditions studied here was a loss of fracture porosity. In addition, CO_2 adsorption in the coal matrix increases the pressure difference between the pore regions and local swelling and leads to a large fracture-matrix compartment interaction. By comparing the porosity changes of both pore regions, it can be inferred that the fracture-matrix interaction plays an important role in the variation of coal porosity and can constrain the temperature effect.

The changes in fracture permeability caused by CO_2 injection are shown in Fig. 15; only the fracture permeability is shown since the fractures provide the principal pathways for fluid flow in coal seams. It can be seen that there is around a 90% reduction of permeability in the vicinity of the injection well relative to the initial permeability. This again highlights the predominant role of CO_2 adsorption-induced coal swelling, which overcomes the competing influence of elevated pore pressures that would tend to increase fracture permeability. Moreover, it has been shown that Joule-Thomson cooling led to a significant drop in temperature under the simulation conditions considered, which further strengthened coal swelling by increasing the CO_2 adsorption capacity.

6. Conclusions

In order to investigate the coupled response of coal to CO_2 injection, this study has presented a coupled thermal, hydraulic and mechanical (THM) model within the framework of dual thermo-poroelastic theory. A numerical solution for the system of governing equations is achieved using the finite element method. Model verification and validation tests have been pursued by comparing the numerical predictions with an analytical solution for a problem of thermo-poroelasticity and experimental results of CO_2 flow through a coal core. The model has then been applied to analyse THM behaviour during CO_2 sequestration in a coal seam.

Under the simulation conditions considered, the numerical results did not indicate a significant distinction between the gas pressures and temperatures in the fracture and coal matrix pore regions, which has been attributed to the input of a relatively small matrix block thickness. As expected, differences between the pressure and temperature of the two pore regions were largest nearer to the injection well and reduced with time and radial flow distance. Despite CO_2 being injected at the same temperature as that of the coal seam, a region of Joule-Thomson cooling was formed, whereby

temperatures in the vicinity of the injection well declined sharply before slowly recovering. The severity of this cooling zone reduced as the CO_2 advanced into the coal seam. CO_2 injection decreased the fracture permeability, especially near the injection well, highlighting the predominance of coal swelling caused by CO_2 adsorption. Moreover, the development of the cooling region further strengthened the coal swelling response since more gas adsorption occurs at lower temperatures. Based on the findings presented in this work, it is recommended that care is taken when assuming isothermal conditions in the computational study of problems of CO_2 sequestration. Whilst the development of a cooling region is not exclusive to the conditions found in coal seams, the temperature change can have a considerable influence on the flow regime due to the coupling with CO_2 adsorption and the associated coal swelling. The influence of non-isothermal behaviour therefore needs to be recognised, especially when making practical plans for CO_2 injection.

Acknowledgments

The first author gratefully acknowledges the financial support provided by the Welsh European Funding Office (WEFO), through the FLEXIS project. The financial support from the China Scholarship Council for the PhD studentship of the second author is also gratefully acknowledged.

References

[1] Thomas H, Hosking L, Sandford R, Zagorščak R, Chen M, An N. Deep ground and energy: carbon sequestration and coal gasification. The International Congress on Environmental Geotechnics: Springer, 2018. p. 38-60.

[2] Sarhosis V, Hosking LJ, Thomas HR. Carbon sequestration potential of the South Wales Coalfield. Environmental Geotechnics. 2016;5(4):234-46.

[3] Busch A, Gensterblum Y, Krooss BM, Littke R. Methane and carbon dioxide adsorption–diffusion experiments on coal: upscaling and modeling. International Journal of Coal Geology. 2004;60(2):151-68.

[4] Zagorščak R, Thomas HR. High-pressure CO2 excess sorption measurements on powdered and core samples of high-rank coals from different depths and locations of the South Wales Coalfield. Energy & Fuels. 2019;33(7):6515-26.

[5] Fan C, Elsworth D, Li S, Zhou L, Yang Z, Song Y. Thermo-hydro-mechanical-chemical couplings controlling CH4 production and CO_2 sequestration in enhanced coalbed methane recovery. Energy. 2019;173(1054-77.

[6] Saliya K, Grgic D, Giot R, Giraud A. Thermo-hydro-mechanical modeling with Langmuir's adsorption isotherm of the CO_2 injection in coal. International Journal for Numerical and Analytical Methods in Geomechanics. 2015;39(6):594-617.

[7] Han WS, Stillman GA, Lu M, Lu C, McPherson BJ, Park E. Evaluation of potential nonisothermal processes and heat transport during CO_2 sequestration. Journal of Geophysical Research: Solid Earth. 2010;115(B7).

[8] Zagorščak R, Thomas HR. Dynamic transport and reaction behaviour of high-pressure gases in high-rank coal. Journal of Natural Gas Science and Engineering. 2019;71(102978.

[9] Oldenburg CM. Joule-Thomson cooling due to CO_2 injection into natural gas reservoirs. Energy Conversion and Management. 2007;48(6):1808-15.

[10] Duru OO, Horne RN. Modeling reservoir temperature transients and reservoir-parameter estimation constrained to the model. SPE Reservoir Evaluation & Engineering. 2010;13(06):873-83.

[11] Chen M, Hosking LJ, Thomas HR. Non-isothermal Gas Flow During Carbon Sequestration in Coalbeds. The International Congress on Environmental Geotechnics: Springer, 2018. p. 113-20.

[12] Ziabakhsh-Ganji Z, Kooi H. Sensitivity of Joule–Thomson cooling to impure CO_2 injection in depleted gas reservoirs. Applied Energy. 2014;113(434-51.

[13] Pan Z, Connell LD. Modelling permeability for coal reservoirs: a review of analytical models and testing data. International Journal of Coal Geology. 2012;92(1-44.

[14] Qu H, Liu J, Pan Z, Peng Y, Zhou F. Simulation of coal permeability under non-isothermal CO_2 injection. International Journal of Oil, Gas and Coal Technology. 2017;15(2):190-215.

[15] Ma T, Rutqvist J, Oldenburg CM, Liu W. Coupled thermal–hydrological–mechanical modeling of CO_2-enhanced coalbed methane recovery. International Journal of Coal Geology. 2017;179(81-91.

[16] Hosking LJ, Thomas HR, Sedighi M. A dual porosity model of high-pressure gas flow for geoenergy applications. Canadian Geotechnical Journal. 2017;55(6):839-51.

[17] Chen M, Hosking LJ, Sandford RJ, Thomas HR. Dual porosity modelling of the coupled mechanical response of coal to gas flow and adsorption. International Journal of Coal Geology. 2019;205(115-25.

[18] Chen M, Hosking LJ, Sandford RJ, Thomas HR. Numerical Analysis of Improvements to CO_2 Injectivity in Coal Seams Through Stimulated Fracture Connection to the Injection Well. Rock Mechanics and Rock Engineering. 2020:1-20.

[19] Jaeger JC, Cook NG, Zimmerman R. Fundamentals of rock mechanics: John Wiley & Sons, 2009.

[20] Peng D-Y, Robinson DB. A new two-constant equation of state. Industrial & Engineering Chemistry Fundamentals. 1976;15(1):59-64.

[21] Chen M. Modelling of gas transport in coal-a hybrid coupled dual porosity and discrete fracture approach. 2019.

[22] Tang X, Ripepi N. Temperature-dependent Langmuir model in the coal and methane sorption process: Statistical relationship. Trans Soc Min Metall Explor. 2016;340(61-9.

[23] Tang X, Li Z, Ripepi N, Louk AK, Wang Z, Song D. Temperature-dependent diffusion process of methane through dry crushed coal. Journal of Natural Gas Science and Engineering. 2015;22(609-17.

[24] Heinze T, Hamidi S. Heat transfer and parameterization in local thermal non-equilibrium for dual porosity continua. Applied Thermal Engineering. 2017;114(645-52.

[25] Hao Y, Fu P, Carrigan CR. Application of a dual-continuum model for simulation of fluid flow and heat transfer in fractured geothermal reservoirs. Proceedings, 38th Workshop On Geothermal Reservoir Engineering, vol SGP-TR-198 Stanford University, Stanford, California2013. p. 462-9.

[26] Liu J, Wang J, Chen Z, Wang S, Elsworth D, Jiang Y. Impact of transition from local swelling to macro swelling on the evolution of coal permeability. International Journal of Coal Geology. 2011;88(1):31-40.

[27] Thomas H, He Y. Analysis of coupled heat, moisture and air transfer in a deformable unsaturated soil. Geotechnique. 1995;45(4):677-89.

[28] Thomas H, Rees S, Sloper N. Three-dimensional heat, moisture and air transfer in unsaturated soils. International Journal for Numerical and Analytical Methods in Geomechanics. 1998;22(2):75-95.

[29] Selvadurai AP, Suvorov A. Thermo-poroelasticity and geomechanics: Cambridge University Press, 2017.

[30] Pini R, Ottiger S, Burlini L, Storti G, Mazzotti M. Role of adsorption and swelling on the dynamics of gas injection in coal. Journal of Geophysical Research: Solid Earth. 2009;114(B4).

[31] Zang J, Wang K, Zhao Y. Evaluation of gas sorption-induced internal swelling in coal. Fuel. 2015;143(165-72.

Figures

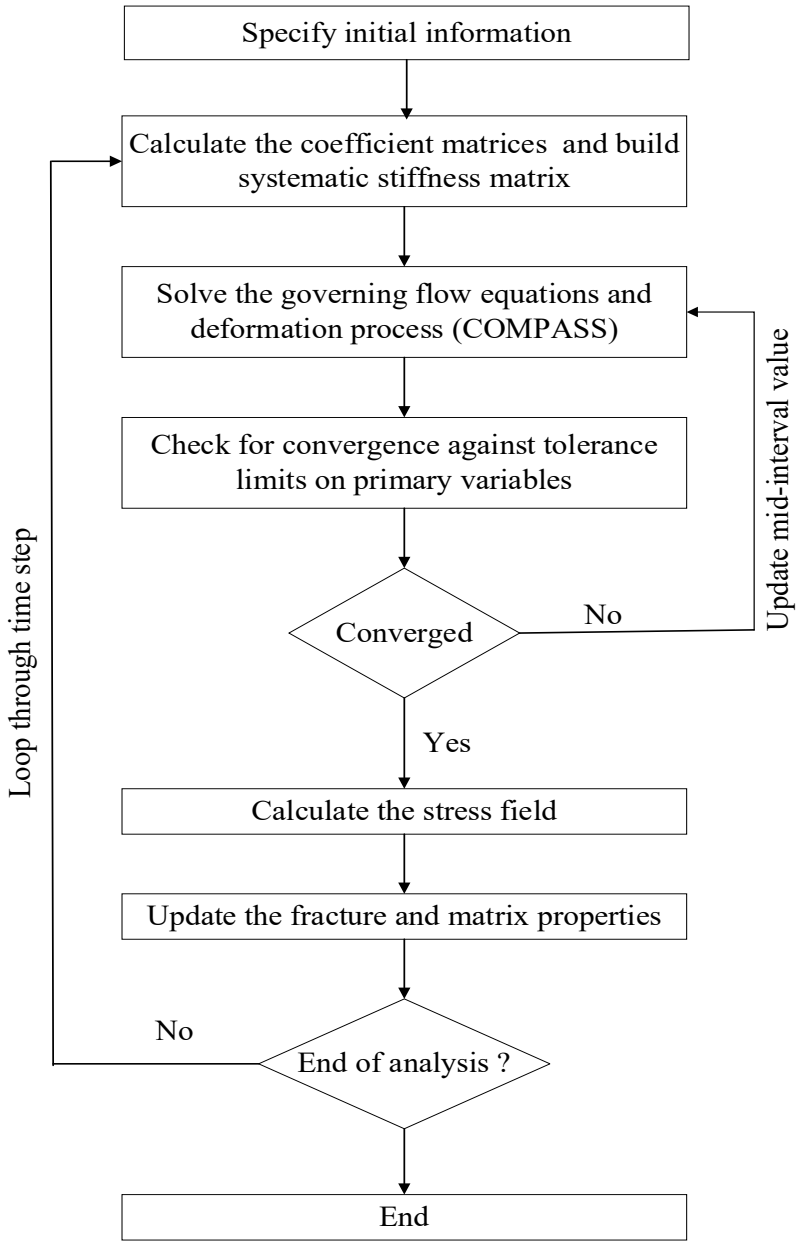

Fig. 1 Numerical solution procedure of the coupled model.

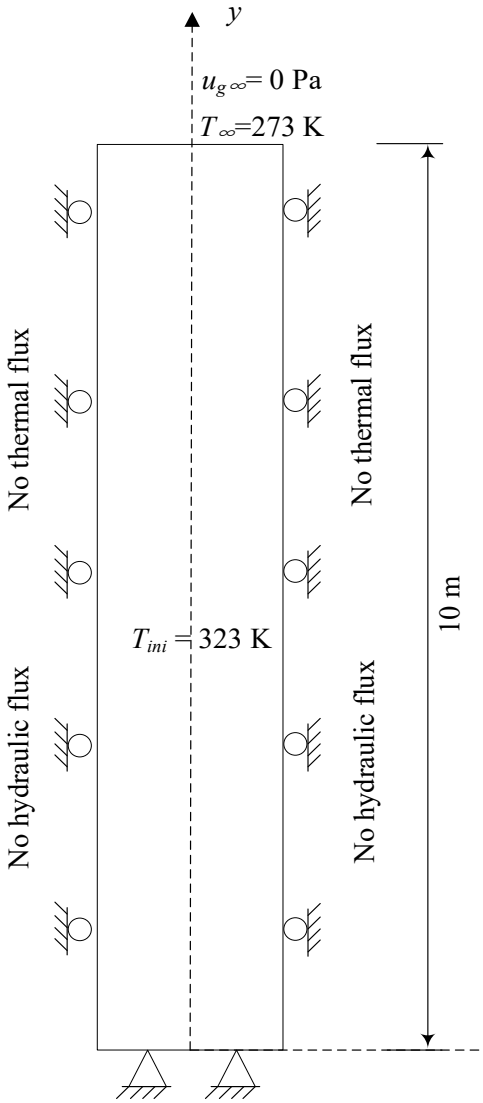

Fig. 2 Schematic of the domain with the initial and boundary conditions used for the verification test.

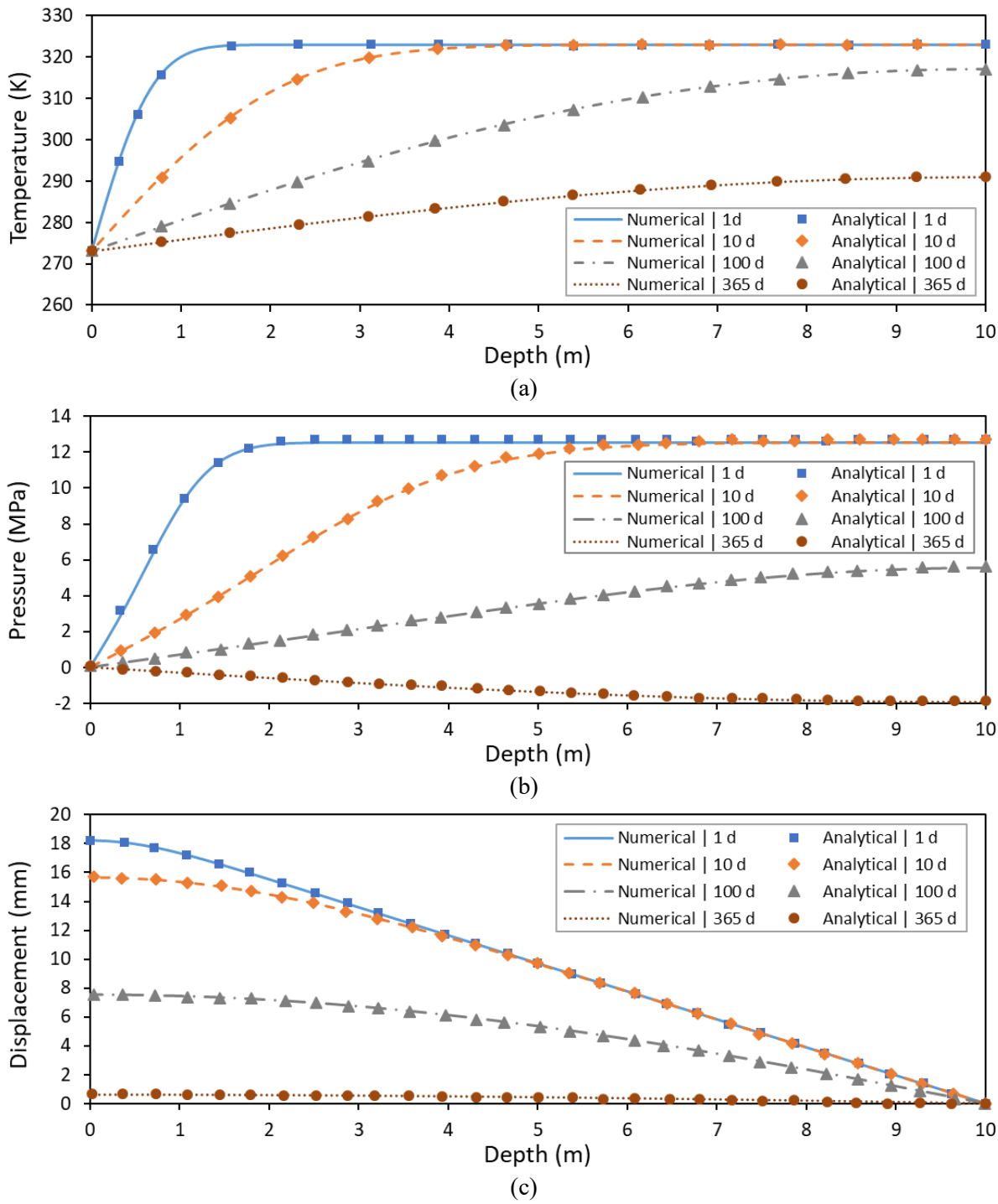

Fig. 3. Comparisons between the numerical results and analytical solutions for (a) temperature, (b) pressure, and (c) displacement.

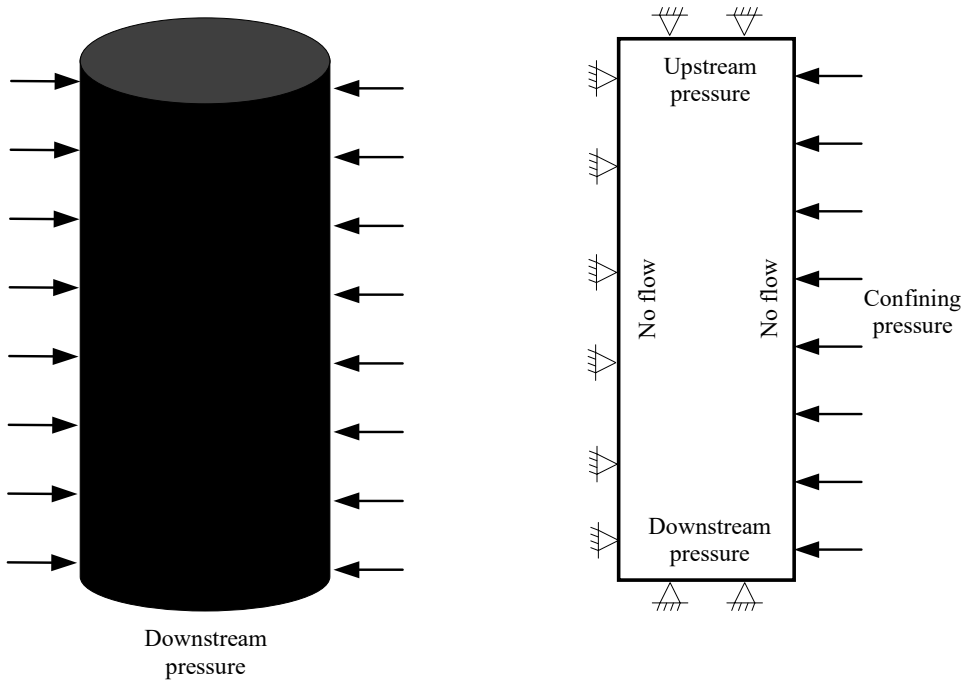

(a) Laboratory coal sample (b) 2D model

Fig. 4 Geometry and boundary conditions for the numerical simulation of an experiment performed by Pini et al. (37).

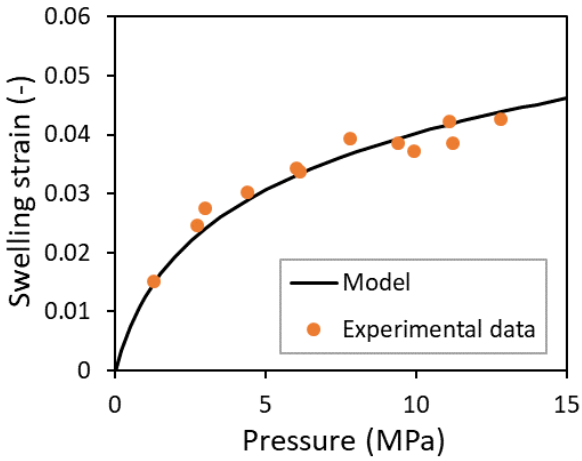

Fig. 5 Comparison of swelling strains predicted by the model with the experimental data.

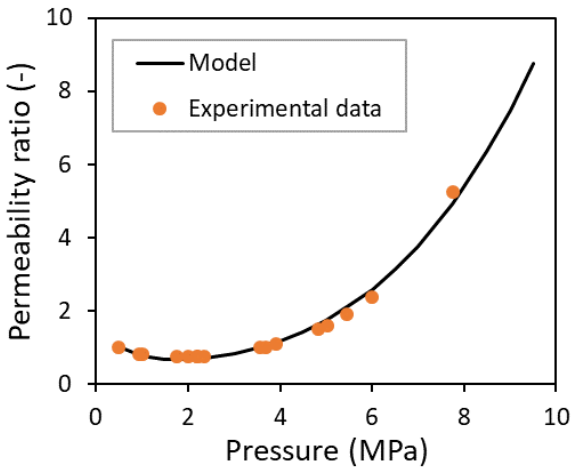

Fig. 6 Comparison of the permeability ratio predicted by the model with the experimental data.

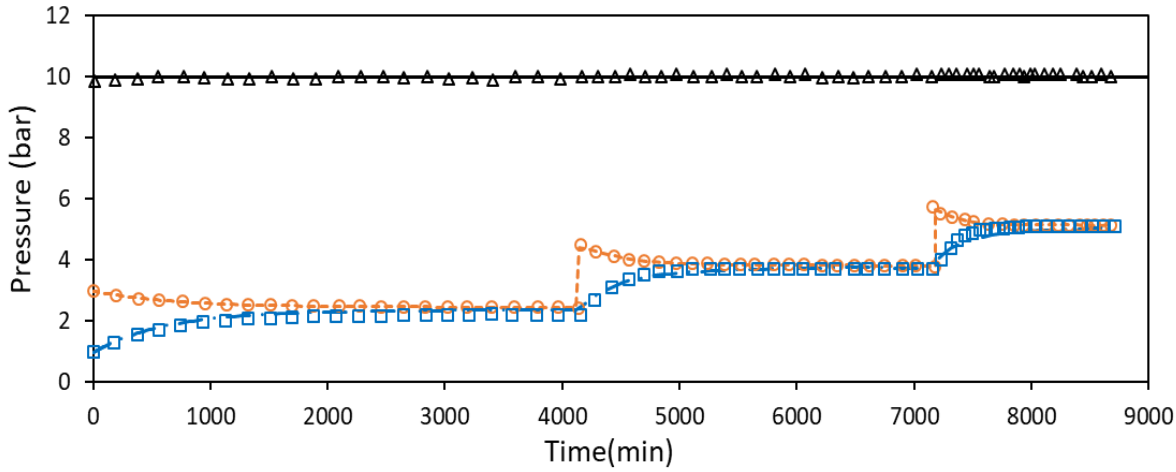

Fig. 7 Comparisons between the predicted results (lines) and experimental measurements (symbols) for the upstream and downstream pressure under a constant confining pressure.

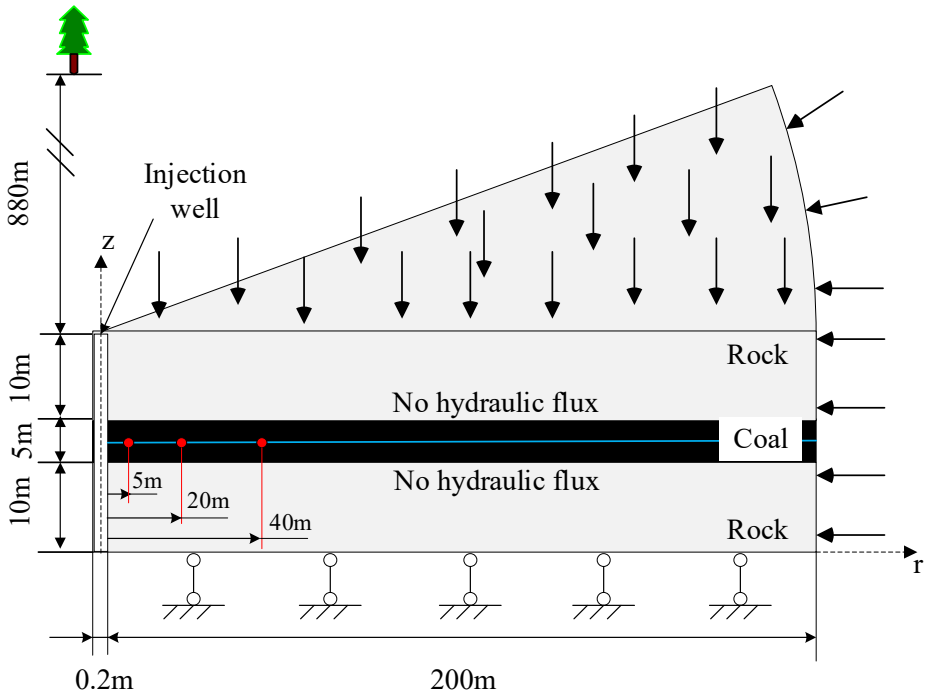

(a)

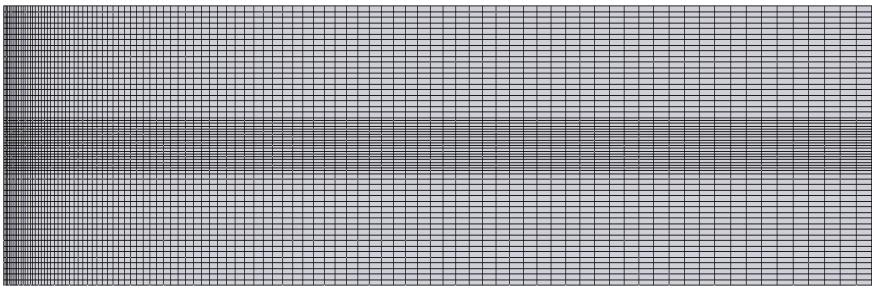

(b)

Fig. 8 (a) Axisymmetric geological model and boundary conditions, and (b) mesh geometry for the numerical analysis performed to analyse coupled THM behaviour during CO_2 sequestration.

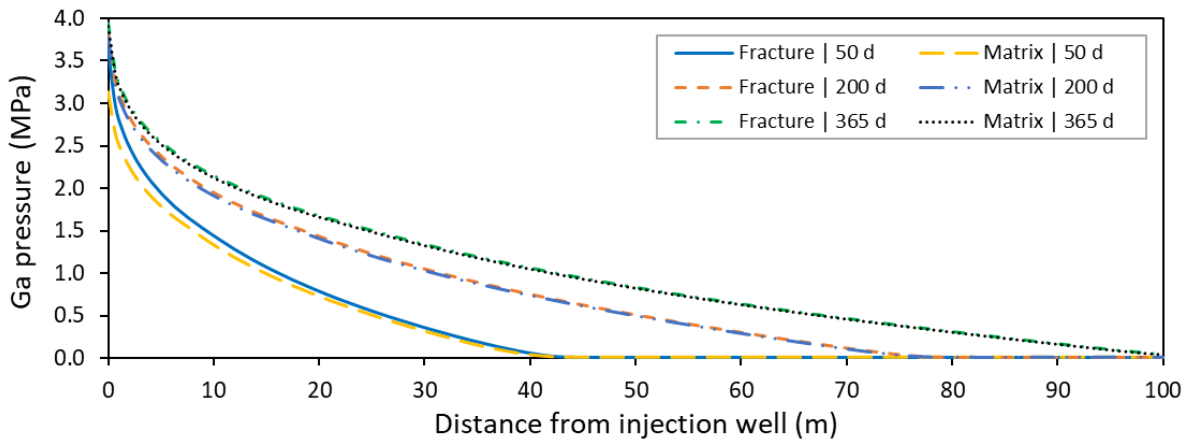

Fig. 9 Radial pressure profiles within the coal seam outward from the injection well at selected times.

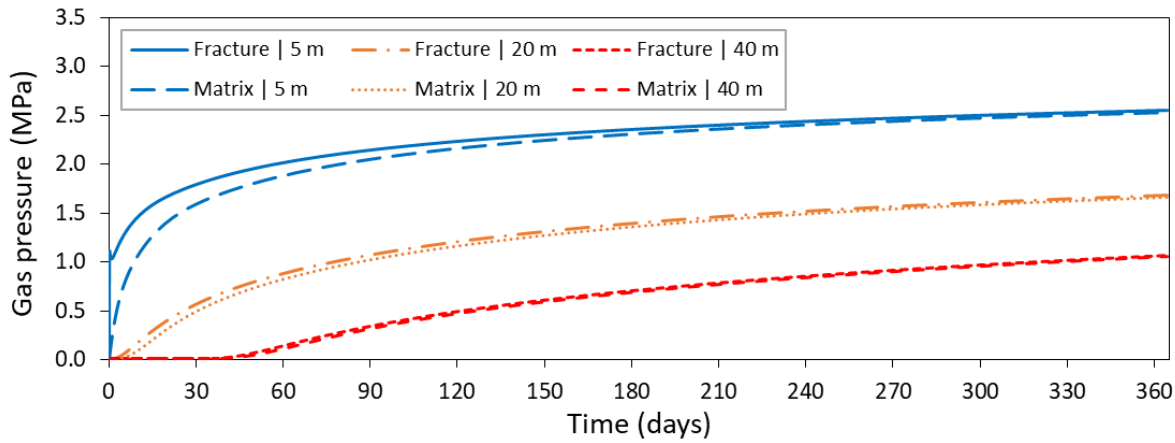

Fig. 10 Temporal change of pressure at radial distances of 5 m, 20 m and 40 m from the injection well.

 doi.org/10.1016/j.ijrmms.2020.104473

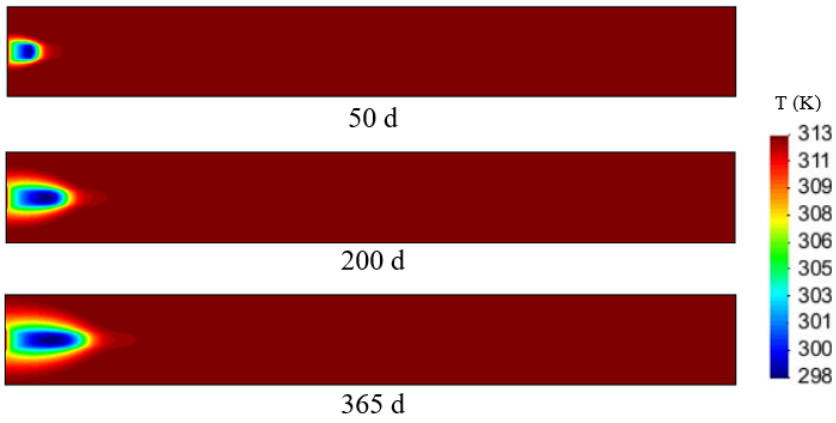

Fig. 11 Radial temperature distribution profiles within the coal seam at selected times.

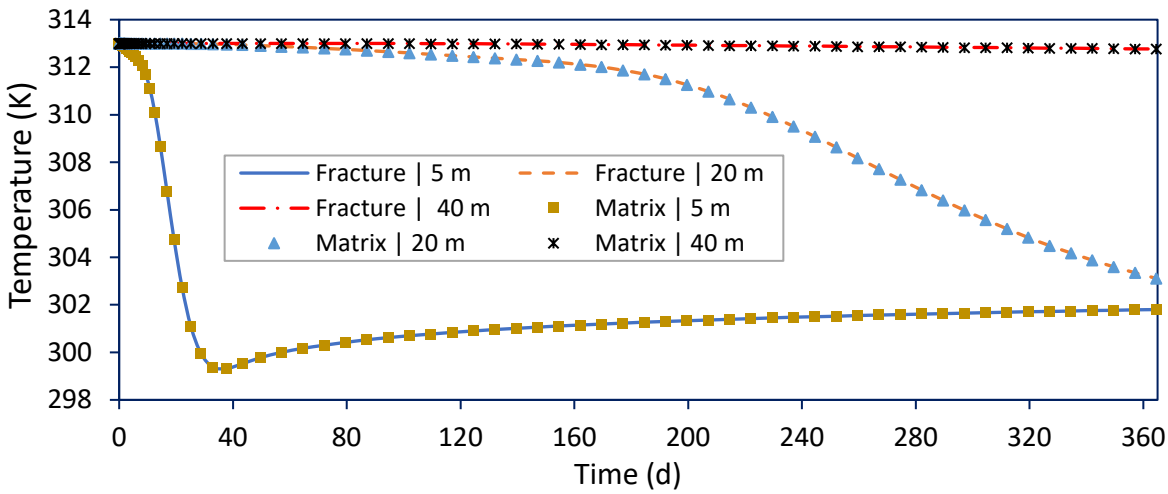

Fig. 12 Temporal change of temperature at radial distances of 5 m, 20 m and 40 m from the injection well.

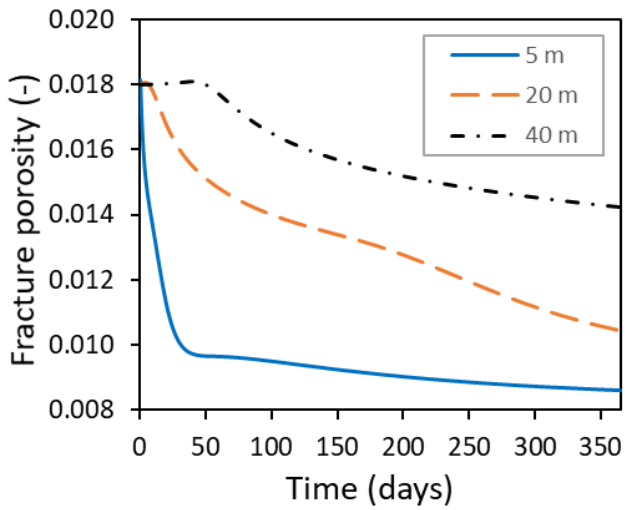

Fig. 13 Temporal changes of fracture porosity at radial distances of 5 m, 20 m and 40 m from the injection well.

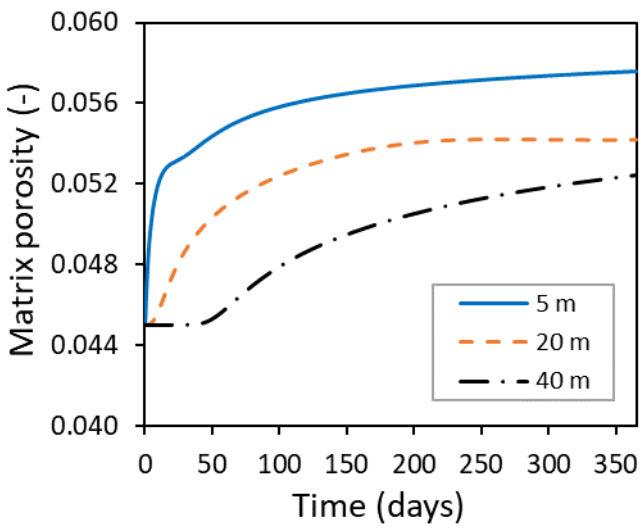

Fig. 14 Temporal changes of matrix porosity at radial distances of 5 m, 20 m and 40 m from the injection well.

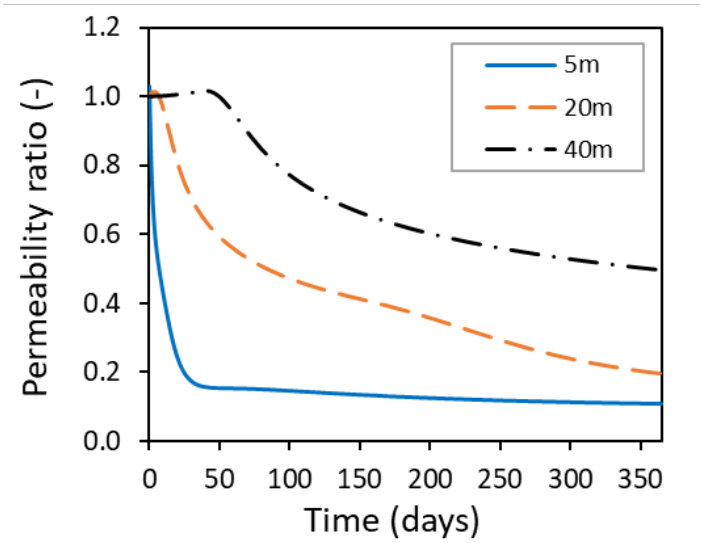

Fig. 15 Temporal changes of fracture permeability at radial distances of 5m, 20 m and 40 m from the injection well.

Tables

Table 1 Material parameters used for the verification test (36).

Material parameters	Value
Bulk modulus, K (GPa)	5
Poisson's ratio, v (-)	0.3
Permeability, k_m (m^2)	6×10^{-19}
Porosity, n_m (-)	0.25
Fluid viscosity, μ (Pa·s)	1×10^{-3}
Modulus of solid constituent, K_s (GPa)	20
Fluid compressibility, C_{cm} (GPa^{-1})	0.4545
Effective thermal conductivity, λ_{em} (W/m/K)	1.62
Effective specific heat capacity, $(\rho C_p)_{eff}$ (J/K/m^3)	1×10^6
Thermal expansion coefficient of solid, α_T (1/K)	8.3×10^{-6}
Thermal expansion coefficient of fluid, α_{Tm} (1/K)	6.9×10^{-5}

Table 2 Material parameters used for the validation test against the experiment by Pini et al. (37).

Material parameters	Value
Young's modulus of coal, E (GPa)	1.12
Matrix modulus, K_m (GPa)	10.34
Poisson's ratio, v (-)	0.26
Initial permeability, k_{f0} (m^2)	1.1×10^{-19}
Initial matrix porosity n_{m0} (-)	0.02
Initial fracture porosity n_{f0} (-)	0.0042
Density of coal, ρ_c (kg/m^3)	1356.6
Viscosity of gas, μ_g (Pa·s)	1.1×10^{-5}
Langmuir volume constant, V_L (mol/kg)	2.49
Langmuir pressure, b_L (MPa^{-1})	1.25
Langmuir strain constant, ε_L (%)	4.9
Sorption time, τ (s)	2.58×10^5
Internal swelling ratio, γ (-)	0.19
Adsorption induced swelling coefficient, $\varphi\Gamma^{max}$ (mol m^{-3})	6.06×10^4
Formation temperature, T (K)	318.15
Gas constant, R (J/mol/K)	8.314

Table 3 Input parameters used for the numerical simulation of CO_2 sequestration in coal.

Material parameters	Value	Reference
Bulk modulus of rock, K (GPa)	6.9	[1]
Poisson' ratio of rock, v (-)	0.21	[1]
Density of rock, ρ_r (kg/m^3)	2450	[1]
Specific heat capacity of rock C_{pr},(J/K/kg)	898	[2]
Thermal conductivity of rock, λ_r (W/m/K)	0.65	[2]
Thermal expansion coefficient of rock, α_T (1/K)	3×10^{-5}	[3]
Bulk modulus of coal, K (GPa)	2.18	[1]
Poisson's ratio of coal, v (-)	0.35	[1]
Bulk modulus of coal matrix, K_m (GPa)	7.65	[4]
Initial permeability of fracture system,k_{f0} (m^2)	3.6×10^{-15}	[1]
Initial porosity of coal matrix, n_{m0} (-)	0.045	[5]
Initial porosity of fracture, n_{f0} (-)	0.018	[5]
Gas viscosity, μ (Pa·s)	1.84×10^{-5}	[6]
Thermal conductivity of CO_2, λ_g (W/m/K)	0.0246	[7]
Density of coal, ρ_c (kg/m^3)	1470	[1]
Thermal conductivity of coal, λ_s (W/m/K)	0.33	[7]
Specific heat capacity of coal, C_{ps} (J/K/ m^3)	1250	[7]
Thermal expansion coefficient of coal, α_T (1/K)	9×10^{-5}	[7]
Maximum adsorption capacity, V_L (mol/kg)	0.91	[1]
Temperature-independent Langmuir constant, $b_{L\infty}$ (1/MPa)	0.89	[1]
Interaction energy, E_i (J/mol)	1197	[8]
Surface stress parameter, $\varphi\Gamma^{max}$ (mol/m^3)	5.7×10^4	-
Ratio of local swelling to global swelling, γ (-)	0.25	Fitting
Sorption time, τ (s)	2×10^5	[9]
Universal gas constant, R (J/mol/K)	8.314	-
Matrix block length, l (m)	0.01	[6]